mathematics

MDPI

Article

Generation of Boxes and Permutations Using a Bijective Function and the Lorenz Equations: An Application to Color Image Encryption

Víctor Manuel Silva-García [1], Rolando Flores-Carapia [1], Manuel Alejandro Cardona-López [2,*] and Miguel Gabriel Villarreal-Cervantes [1]

[1] Instituto Politécnico Nacional, IPN-CIDETEC, Ciudad de México 07738, Mexico
[2] Instituto Politécnico Nacional, Centro de Investigación en Computación, Ciudad de México 07738, Mexico
* Correspondence: mcardonal2022@cic.ipn.mx

Abstract: Some images that contain sensitive information and travel through the network require security. Therefore, a symmetric cryptosystem that encrypts images and resists known attacks is developed. Subsequently, in this work, an encryption algorithm known as Image Cipher utilizing Lorenz equation and a Bijective Function—ICLEBF are proposed. In the proposal, the Lorenz equations and the Bijective function are used to generate boxes, the permutation, and schedule keys, considering that all these elements are different in each encryption process. The encryption procedure consists of 14 rounds, where a different box is applied in each round. In this type of algorithm, the impact of quantum computers will be less forceful and can be useful for that epoch. On the other hand, the quality of the encrypted images and the loss of sharpness in decoded images with damage are measured. In addition, an attack from five types of noise (one of which is a developed proposal) is carried out by applying it to encrypted images. Finally, the results of the proposed ICLEBF are compared with other recent image encryption algorithms, including the Advanced Encryption Standard. As a result, this proposal resists known attacks and others that the current standard does not support.

Keywords: Lorenz equations; bijective function; dynamic *S*-box; dynamic permutation; noise in encrypted images

MSC: 11T71

Citation: Silva-García, V.M.; Flores-Carapia, R.; Cardona-López, M.A.; Villarreal-Cervantes, M.G. Generation of Boxes and Permutations Using a Bijective Function and the Lorenz Equations: An Application to Color Image Encryption. *Mathematics* **2023**, *11*, 599. https://doi.org/10.3390/math11030599

Academic Editors: Theodore E. Simos and Charampos Tsitouras

Received: 12 December 2022
Revised: 11 January 2023
Accepted: 20 January 2023
Published: 24 January 2023

1. Introduction

Large amounts of sensitive information can be sent over the network using images leading to the development of robust encryption systems employed to encrypt them [1–5]. In the same way, Lorenz equations have been widely applied in the different design stages of cryptosystems for image ciphering [6–9]. In this research, a fourteen-round symmetric algorithm is proposed, that is based on the Lorenz equations and the bijective function. Furthermore, the distribution of keys and signs is based on the elliptic curve [10].

Regarding the security of the ICLEBF cryptosystem, three aspects are studied. First, the security of the proposed symmetric cryptosystem is analyzed according to known attacks such as differential, linear, algebraic, and brute force. For example, the differential attack is evaluated according to the following parameters: Number of Pixels Change Rate (NPCR), Unified Average Changing Intensity (UACI), and Avalanche Criteria (AC) [11]. In addition, it must be taken into account that both the boxes and the permutation involved in the encryption are different in each process; that is, they are variables [12].

Regarding the second aspect, the encrypted images are damaged using five types of noise. The five noises are: additive, multiplicative, Gaussian, occlusion, and a noise that is related to the Chi-Square (χ^2) distribution. A median filter of 5×5 is also applied to

the damaged decrypted images to complement the process and improve their sharpness. On the other hand, images decoded with noise are evaluated according to a parameter that the authors refer to as the Similarity Parameter (SP). The SP parameter is proposed in this research to evaluate the loss of sharpness in damaged images. The resistance of the proposed algorithm to noise attacks with respect to the AES–CBC [13] cryptosystem is also compared and analyzed.

The third aspect involves an attack on the elliptic curve that is included in the proposal to distribute the keys of the symmetrical system, resulting in the discrete logarithm problem [14]. This point is addressed by comparing the discrete logarithm attack with the factorization of a natural number n having two prime factors, p, q, each of which has approximately the same number of digits [15].

The generation of schedule keys is carried out by randomly choosing a point on the elliptic curve and the Lorenz equations. Furthermore, according to another randomly generated point on the curve, and using a bijective function that goes from the set of non-negative integers to the set of permutations [15], the boxes involved in each round are built; plus, a permutation of the image size. Note that a S-box 8×8 is a permutation of 256 elements.

The quality of the encrypted images is measured according to the following elements: entropy, three-way correlation, discrete Fourier transform, energy, homogeneity, contrast, NPCR, UACI, AC, and a goodness-of-fit test using the χ^2 [16]. In some countries, compression with loss of information is not accepted; for instance, in Mexico [17], the images have to accomplish a 512×512 pixel size in BMP format. In addition, the ICLEBF cryptosystem was developed for software implementation in Java.

The present work is organized as follows: Section 2 presents the tools that are employed in this research. Section 3 presents the construction of the elements involved in the encryption algorithm and the test images. Section 4 shows the construction of different noises and their application to encrypted images. In addition, a high-level description of the median filter 5×5 and the SP parameter is made. The results are shown in Section 5, and their analysis and discussion are presented in Section 6. Finally, Section 7 presents the conclusions and future work.

2. Materials and Methods

A high-level description of the tools required in the proposal is presented in the next section.

2.1. Elliptic Curve

ICLEBF is a symmetric cryptosystem based on two points on the elliptic curve and the use of the Lorenz equations. Therefore, it is convenient to provide a general description of the elements used to generate the elliptic curve. First, the equation of the discrete elliptic curve is written in Equation (1):

$$y^2 \equiv x^3 + ax + b \mod p \tag{1}$$

This work uses a prime number p greater than 2^{512}. The prime p is related to the equation $p = a_1^2 + a_2^2$ considering a_1 as an odd number, a_2 as an even number, $p \mod 4 \equiv 1$, and $(a_1 + a_2) \mod 4 \equiv 1$. Set the constant $b = 0$ and $a = -k$, the Equation (1) results in Equation (2).

$$y^2 \equiv x^3 - kx \mod p \tag{2}$$

On the other hand, the constant k must satisfy that $k^{p-1/2} \bmod p \equiv 1$ and $k^{p-1/4} \bmod p \not\equiv 1$ [18]. In addition, the proposed elliptic curve must meet certain conditions to avoid cryptanalysis attacks known as the MOV attacks or to generate a trace one curve since the latter is considered weak [19]. The conditions are presented in Equations (3) and (4).

$$\#E(F_q) \not\equiv 1 \mod p \tag{3}$$
$$\#E(F_q) \neq p \tag{4}$$

where $q = \frac{p + 2a_1 + 1}{4}$ must be a prime number and $\#E(F_p) = p + 2a_1 + 1$ represents the total number of solutions of the curve [20]. If q does not result in a prime number, the prime number q must be changed.

On the other hand, the curve's equation must have three different real roots (non-singular solutions). This requirement is expressed in Equation (5).

$$4((-k)^3) \not\equiv 0 \mod p \tag{5}$$

It is possible to generate a curve that meets all these requirements by using an algorithm [21]. It is pointed out that in the solution set of the curve, it is possible to define the addition operation (+), which makes this set an abelian group [22].

In the calculation of the sums, the operation of the multiplicative inverse module p is used. This operation is performed using Euclid's extended algorithm [23]. However, it is possible to perform the calculations differently to reduce execution times. In Section 3, we will prove a theorem and propose an algorithm for calculating the multiplicative inverse.

Since the number of solutions q is prime, then there are some elements in the solution set that generate all the others, i.e., any point P of the solution set can be written as $P = k\alpha$, where α is the generator element [24]. In fact, a curve is defined if k, p, q, and α are known.

To conclude this section, an example is provided below:

Example. Given a_1 = 341 and a_2 = 40, it follows that p is 117881. It can be verified that p mod 4 $\equiv$ 1, and $a_1 + a_2 \equiv 1$ mod 4. A primitive element is selected, namely α = (95360, 92352), and k value is given by k = 85264. Then, k is verified using Equations (6) and (7). Therefore the resulting curve is: $y^2 \equiv x^3 - 85264x \mod 117881$.

$$(85264)^{117881-1/4} \mod 117881 \not\equiv 1 \tag{6}$$
$$(85264)^{117881-1/2} \mod 117881 \equiv 1 \tag{7}$$

To verify the primitive element α, it must meet that $(q-1)[\alpha = (x, y)] = (x, -y)$. In this case, we have $(29641 - 1)(95360, 92352) = (95360, -92352)$, taking into account that $q = 29641$. The total number of solutions is $\#E(F_{117881}) = 118564$. In addition, it meets the following conditions: 29641 mod 117881 $\not\equiv 1$, $4(-85264)^3$ mod 117881 $\not\equiv 0$ and $\#E(F_{29641}) \neq 117881$. So, the curve is not supersingular, not singular and neither trace one.

2.2. Lorenz Equations

The Lorenz equations describe the atmospheric phenomenon of convection, and they are expressed according to Equations (8)–(10) [7].

$$\dot{x} = \tau(-x + y) \tag{8}$$
$$\dot{y} = rx - y - xy \tag{9}$$
$$\dot{z} = -bx + xy \tag{10}$$

The critical points are obtained when Equations (8)–(10) are equal to zero. Furthermore, the values τ, r, and b are considered positive real numbers. From here, it is not difficult to obtain the following critical points: $Q_1 = (0, 0, 0)$, $Q_2 = (\sqrt{b(r-1)}, \sqrt{b(r-1)}, r-1)$ y $Q_3 = (-\sqrt{b(r-1)}, -\sqrt{b(r-1}, r-1)$.

In this investigation, the values $\tau = 10$ and $b = 8/3$ are chosen. The solution to this system of equations is written as in Equation (11).

$$\vec{X} = \vec{\xi} e^{\lambda t} \tag{11}$$

Considering that the Lorenz equations describe the phenomenon of convection in the Earth's atmosphere, the following parameters are set as: $\sigma = 10$ and $b = \frac{8}{3}$. The solution to the Lorenz system of equations has the form $\vec{X} = \vec{\xi} e^{\lambda t}$ where $\vec{\xi}$ represents the eigenvectors, and λ the eigenvalues.

On the other hand, to calculate the solutions in the neighborhood of the point Q_2, we start from the equation where the matrices B, X and $X^{'}$ are described in Equations (12), (13) and (14), respectively.

$$B = \begin{pmatrix} 10 & 10 & 0 \\ r & -1 & -\sqrt{8/3(r-1)} \\ \sqrt{8/3(r-1)} & \sqrt{8/3(r-1)} & -8/3 \end{pmatrix} \tag{12}$$

$$X = \begin{pmatrix} \mathrm{x} \\ \mathrm{y} \\ \mathrm{z} \end{pmatrix} \tag{13}$$

$$X^{'} = \begin{pmatrix} x' \\ y' \\ z' \end{pmatrix} \tag{14}$$

The eigenvalues are calculated from the characteristic polynomial, which is obtained from Equation (15).

$$|B - \lambda I| = 0 \tag{15}$$

Considering that the parameter $r = 28$, the characteristic polynomial is expressed in Equation (16).

$$3\lambda^3 + 41\lambda^2 - 50\lambda + 2160 = 0 \tag{16}$$

From Equation (16), one real root and two complex ones are obtained; these are written in Equations (17)–(19).

$$\lambda_1 = -22.558424 \tag{17}$$

$$\lambda_2 = 4.445878 + 3.485904i \tag{18}$$

$$\lambda_3 = 4.445878 - 3.485904i \tag{19}$$

Regarding the eigenvectors, it is only necessary to generate two of them to obtain the general solution. Equations (20) and (21) show the eigenvectors $\vec{\xi_1}$ and $\vec{\xi_2}$, where $c = 4.445878$.

$$\vec{\xi_1} = \begin{pmatrix} 9.163288 \\ -11.507650 \\ 1 \end{pmatrix} \tag{20}$$

$$\vec{\xi_2} = \begin{pmatrix} 0.359510 + 0.116796i \\ 0.478680 + 0.294040i \\ 1 + 0i \end{pmatrix} \tag{21}$$

$$\vec{u(t)} = \begin{pmatrix} 0.3595\cos(3.4859)t - 0.1167\sin(3.4859)t \\ 0.4786\cos(3.4859)t - 0.2940\sin(3.4859)t \\ \cos(3.4859)t \end{pmatrix} e^c \tag{22}$$

$$\vec{v(t)} = \begin{pmatrix} 0.1167\cos(3.4859)t - 0.3595\sin(3.4859)t \\ 0.2940\cos(3.4859)t - 0.4786\sin(3.4859)t \\ \sin(3.4859)t \end{pmatrix} e^{c} \tag{23}$$

Note that the solution $\vec{\xi_2}e^{(4.445878+3.485904i)t}$ contains a real part and a complex part. The real part is presented as $\vec{u}$ and the complex one as $\vec{v} \times i$, where $\vec{u}$ and $\vec{v}$ are expressed in Equations (22) and (23). Furthermore, if we set $\vec{w} = \vec{\xi_1}e^{-22.5584t}$, the general solution is then written in Equation (24).

$$\vec{X(t)} = e^{-22.5584t}D_1\vec{\xi_1} + D_2\vec{u}(t) + D_3\vec{v}(t) \times i \tag{24}$$

In this work, the second coordinate of vectors that appear in Equation (24) is taken, resulting in $\phi_y(t)$. Considering that the constant D_1 of the general solution becomes equal to zero, and the variable t takes the value $t_1 = 1/4.445878$, $\phi_y(t_1)$ results in Equation (25).

$$\phi_y(t_1) = (0.4750)D_2e + (0.2881)D_3e \tag{25}$$

In practice, although a finite sequence of decimals is taken, this does not imply that the conditions of Chaos are not met.

2.3. Correlation Coefficient

The correlation coefficient, or simply correlation, is calculated in three directions. The correlation parameter is a measure of the figure quality; furthermore, it is used in many works of this kind of research [25,26].

The procedure to carry out this measurement is explained next: m pixels are randomly selected from the encrypted image. Subsequently, for each one of them, the pixels adjacent to it are taken, that is, in the horizontal, vertical, and diagonal directions. For example, suppose we want to analyze the vertical direction for the color green. So, each of these m pixels has the green color, which ranges from the values 0 to 255, denoting this value as x_g. Next, the adjacent pixel in the vertical direction is taken. This pixel has the green color with a certain level that varies in the same way as the previous one. Therefore, let us call it y_g.

Hence, the formulas to calculate the correlation in the vertical direction for the green color are presented in the Equation (26). The terms $\overline{x}_g$, $\overline{y}_g$ are the averages of x_g and y_g, and their calculations are shown in Equations (27) and (28).

$$r_{v;x_g,y_g} = \frac{\frac{1}{m}(\sum_{i=1}^{m}(x_{i,g} - \overline{x}_g)(y_{i,g} - \overline{y}_g))}{\sqrt{(\frac{1}{m}\sum_{i=1}^{m}(x_{i,g} - \overline{x}_g)^2(\frac{1}{m}\sum_{i=1}^{m}(y_{i,g} - \overline{y}_g)^2))}} \tag{26}$$

$$\overline{x}_g = \frac{1}{m}\sum_{i=1}^{m} x_{i,g} \tag{27}$$

$$\overline{y}_g = \frac{1}{m}\sum_{i=1}^{m} y_{i,g} \tag{28}$$

The calculation of the correlation in the other directions and colors is very similar.

2.4. Entropy

Another parameter useful to evaluate the encrypted images is the information entropy [27]. This parameter is measured according to Equation (29) [28]. In addition, it is pointed out that this measurement is carried out for each primary color in the case of encrypted images.

In this same order of ideas, it is mentioned that each primary color in an encrypted image is described by 256 levels, represented by a byte. The primary colors are: red, green and blue. From here, an image is well encrypted if the entropy of each color is close to 8. It is pertinent to clarify that this condition is necessary but not sufficient because the

distribution of information can have entropy 8, and the information cannot have a random distribution [18].

$$H(x) = -\sum_{x\varepsilon X} P(x) log_2 P(x) \tag{29}$$

On the other hand, it is pointed out that entropy is not the only parameter used to evaluate encrypted images. In practice, an entropy value close to 8 is associated with a good randomness [29].

2.5. Discrete Fourier Transform

This test is part of the NIST 800-22 [30] standard. It evaluates that there are no repeating patterns in a binary string, which means that it is random. Furthermore, it can be stated that it is a statistical hypothesis test, where the null hypothesis is that the binary string is random, against the alternative one that it is not.

On the other hand, the variables that intervene in this procedure are expressed below.

N_0 is a quantity obtained according to Equation (30), where m represents the chain length of zeros and ones.

The function f_j is defined in the Equation (31) where i is the complex number $\sqrt{-1}$, and the variable x_k is equal to ± 1.

Once the function f_j is defined, the variable N_1 is determined as the number of times that $\|f_j\|$ is less than the value h; considering that it is defined as: $h = \sqrt{\mathrm{Ln}\frac{1}{0.05}(m)}$.

Taking into account the variables N_0, N_1; the variable d is represented in Equation (32).

On the other hand, the function $erfc\frac{|\ d\ |}{\sqrt{2}}$ is represented in Equation (33). Based on the above, the decision rule $P - value = erfc\frac{|\ d\ |}{\sqrt{2}}$ is defined as follows:

If $P - Value > 0.01$, the null hypothesis is accepted; that is, the string of zeros and ones is random; otherwise, it is rejected.

$$N_0 = (0.95) \times m/2 \tag{30}$$

$$f_j = \sum_{k=1}^{m} x_k e^{\frac{2\pi(i)(k-1)j}{n}} \tag{31}$$

$$d = \frac{N_1 - N_0}{\sqrt{\frac{n(0.95)(0.05)}{4}}} \tag{32}$$

$$\mathrm{erfc}\frac{|\ d\ |}{\sqrt{2}} = 2(1 - \Phi(|\ d\ |)) \tag{33}$$

2.6. Goodness-of-Fit Test

This tool is a statistical hypothesis test, where the null and alternative hypotheses are as follows:

(I) Null hypothesis. The string of bits is random.

(II) Alternative hypothesis. The string of bits is not random.

In addition, it is necessary to define a statistic and a level of significance, which in this investigation is $\alpha = 0.01$ [31], that determines a region of acceptance or rejection and, subsequently, the decision rule.

The statistic is shown in Equation (34), which has a χ^2 distribution with $n - 1$ degrees of freedom. Regarding the variables involved in Equation (34), it is noted that o_i, exp correspond to the observed and expected values. Furthermore, considering that each primary color is described with 256 levels (a byte), we conclude that the degrees of freedom are $n - 1 = 255$. With this argument, and in accordance with the central limit theorem,

in this paper we assume that the variable χ^2 approximates a normal distribution $N(\mu, \sigma)$; where $\mu = 255$ and $\sigma = 22.58$ [32].

$$\chi^2 = \sum_{i=1}^{k} \frac{(o_i - \exp)^2}{\exp} \tag{34}$$

On the other hand, according to the significance level value defined above, it follows that when $\chi^2 < 308$, the null hypothesis is accepted. On the contrary, it is rejected if $\chi^2 \geq 308$.

Furthermore, it is mentioned that the measurement of the encrypted image quality is carried out for each primary color; red, green, and blue. In addition, it is pointed out that this type of test is not found in the NIST 800-22.

2.7. Parameters NPCR, UACI and AC

In this research, three parameters are used to measure the strength of ICLEBF to differential attacks and the quality of encryption. These parameters are: NPCR, UACI, and AC.

Equation (35) describes the NPCR parameter, where the subscript c indicates the primary color; red, green, or blue. Regarding the elements that intervene in it, it is mentioned that the function $D(i, j)$ proceeds as follows: it is equal to 1 when the bytes in position (i, j) of the encrypted images have the same value. On the contrary, it presents a zero value when they are different. It is important to point out that the flat images are only different by one byte. The variables W, H represent the width and height of the image. The value considered appropriate for this parameter is a percentage close to 99.6% [33].

$$\text{NPCR}_c = \frac{\Sigma_{i,j} D(i, j)_c}{W \times H} \times 100\% \tag{35}$$

Equation (36) describes the value of UACI, considering that the variable $C(i, j)_{l,c}$ is in a range from 0 to 255 and corresponds to the l-th encrypted images. As commented before, the flat images are only different by one byte. On the other hand, (i, j) and c correspond to the byte position and the primary color.

The value considered adequate for this parameter is 33.4% [34].

$$\text{UACI}_c = \frac{1}{W \times H} [\Sigma_{i,j} \frac{\mid C_{1,c} - C_{2,c} \mid}{255}] \times 100\% \tag{36}$$

Equation (37) describes the parameter AC, where the function $b(i, j)$ is equal to 1 when the pixels of images related to the position (i, j) are the same. Otherwise, $b(i, j)$ is equal to 0. The variable T represents the number of bits in the image. Likewise, to resist the differential attack, it is considered that AC is close to 50% [35]. In addition, the subscript c indicates the type of primary color that is analyzed.

$$\text{AC}_c = \frac{\Sigma_{i,j} b(i, j)_c}{T} \times 100\% \tag{37}$$

2.8. Parameters of Homogeneity, Contrast, Energy and Median Filter

In many image encryption investigations, Contrast, Homogeneity, and Energy parameters are used to assess the quality of encryption. Each of them is briefly described below.

Regarding Homogeneity, it is evaluated with Equation (38), considering that (i, j) are the coordinates of the pixel and $g(i, j)$ its value at that position. On the other hand, an image is said to be "well" encrypted when the Homogeneity values are small, i.e., the smaller the Homogeneity value, the higher the quality of the encryption obtained [36].

$$\textit{Homogeneity} = \sum_{i,j} \frac{g(i, j)}{1 + \mid i - j \mid} \tag{38}$$

Equation (39) represents the Contrast parameter, which measures the degree of inequality between a pixel and its neighbors. We then say that the encryption of an image is "good" if the contrast values are large. In the results section, the obtained values are compared with other investigations [37]. The function $g(i,j)$ provides the value of g in the pixel (i,j).

$$Contrast = \sum_{i,j} \mid i-j \mid^2 g(i,j) \tag{39}$$

The third parameter, Energy, is evaluated according to Equation (40). This parameter measures the degree of disorder between the pixels. The closer this value is to zero, the greater the disorder, which implies that the encryption is "good" [38].

$$Energy = \sum_{i,j} g(i,j)^2 \tag{40}$$

2.9. Median Filter

It is clear that when damage is inflicted upon the encrypted image, there will be a loss of sharpness in the decrypted image. Therefore, improving the sharpness of the decrypted image with damage is convenient and thus complements this process. This represents the motivation in this work to use a median filter 5×5 [39]. In this sense, a filter manipulates neighboring pixels of size $(n \times m)$ in a general perspective.

Hence, the median filter 5×5 proceeds as follows: given any pixel (x_1, x_2) of the image map, a mask of 25 pixels is constructed, leaving the point (x_1, x_2) in the center, and the other pixels as its neighbors. Table 1 illustrates this aspect.

Table 1. A mask of 5×5 for the median filter.

(x_1-2, x_2+2)	(x_1-1, x_2+2)	(x_1, x_2+2)	(x_1+1, x_2+2)	(x_1+2, x_2+2)
(x_1-2, x_2+1)	(x_1-1, x_2+1)	(x_1, x_2+1)	(x_1+1, x_2+1)	(x_1+2, x_2+1)
(x_1-2, x_2)	(x_1-1, x_2)	(x_1, x_2)	(x_1+1, x_2)	(x_1+2, x_2)
(x_1-2, x_2-1)	(x_1-1, x_2-1)	(x_1, x_2-1)	(x_1+1, x_2-1)	(x_1+2, x_2-1)
(x_1-2, x_2-2)	(x_1-1, x_2-2)	(x_1, x_2-2)	(x_1+1, x_2-2)	(x_1+2, x_2-2)

From here, it is possible to order these 25 values according to their intensity, and then the value that meets the following requirement is chosen as the median: it is greater than or equal to the first $\lceil \frac{25}{2} \rceil - 1$ element, i.e., the 50%, and less than the remaining points.

Because in this investigation the analysis is carried out for each of the primary colors (red, green and blue), the median of each of these colors are then denoted as follows: $M_{r,(x_1,x_2)}$, $M_{g,(x_1,x_2)}$ and $M_{b,(x_1,x_2)}$, respectively.

Finally, the intensity value of each of the mask points is replaced by the median value.

3. Model Development

In this section, the theorem to compute the multiplicative inverse of a number when the modulus is prime, the encryption algorithm, and the generations of permutations and boxes using an algorithm that defines a bijective function [21] are described.

3.1. Calculation of the Multiplicative Inverse

The multiplicative inverse modulo p is used by following the next theorem:

Theorem 1. *Given a prime number p, and an element $x \epsilon Z_p$ such that $x \neq 0$, then the multiplicative inverse modulo p of x is calculated as: $x^{p-2} \mod p$.*

Proof of Theorem 1. Since p is prime, the greatest common divisor (gcd) $\gcd(x, p) = 1$. So, it is stated that x has an inverse, and it is also unique.

From here,

$$x^{p-2} \times x = x^{p-1} \mod p$$

However, $x^{p-1} \mod p \equiv 1$. According to Lagrange theorem [40] and considering that Euler's ϕ satisfies $\phi(p) = p - 1$, then, x^{p-2} is the multiplicative inverse of x. □

The advantage of computing the multiplicative inverse modulo p according to Theorem 1 is that this process is parallelizable [40], in contrast to Euclid's algorithm, whose procedure for calculating the inverse is sequential.

3.2. SP Parameter

The SP parameter is proposed to evaluate the loss of sharpness in the decrypted images with damage. This parameter is represented by Equation (41), where the subscript c indicates the primary color type.

$$\mathrm{SP}_c = |100 - \mathrm{UACI}_c(2.994)| \tag{41}$$

In this work, the UACI instrument defined in Equation (36) is used to produce SP, taking into account the following argument.

Because UACI evaluates the differences $\mid C_{1,c} - C_{2,c} \mid$ between two images, which in this case would be the original and the decrypted with damage, it can be seen that when the two images are the same, UACI = 0, and therefore, SP = 100; however, if UACI $\approxeq$ 33%, which happens when the image is well encrypted, it follows that SP $\approxeq 0$. The factor 2.994 indicates the range of SP from 0 to 100.

So, the parameter SP provides information about the degree of similarity between two images.

3.3. Algorithm for the Generation of Permutations

Given a positive integer n, the following set is defined: $Z_n = \{m \in N \mid 0 \leq m \leq n! - 1\}$. Any element of Z_m can be expressed according to Equation (42). That is, express it on a factorial basis.

$$m = A_0(n-1)! + A_1(n-2)! + \ldots A_{n-2}(1)! + A_{n-1}(0)! \tag{42}$$

On the other hand, according to the division algorithm, the A_i are unique. Moreover, that $A_{n-1} = 0$. Thus, the values A_i satisfy Equation (43).

$$0 \leq A_i < (n - i) \text{ with } 0 \leq i \leq (n - 2) \tag{43}$$

Recent research uses the above arguments to develop an algorithm that builds permutations in a set of n different elements [21]. In this paper, this set is $\{0, 1, \cdots n - 1\}$.

Furthermore, it is shown that the algorithm defines a bijective function [41]. The latter is highlighted because it is convenient that there are two different permutations for two positive integers $m_1, m_2 \in Z_n$. The above allows for building dynamic permutations and boxes for a cryptosystem.

3.4. Cipher Procedure

The high-level description of the ICLEBF cryptosystem consists of a 14-round symmetric encryption algorithm [42]. In this algorithm, both the permutations, the 8×8 *S*-box, and the schedule keys are dynamic, i.e., in each encryption procedure, they are different. Furthermore, the size of permutations and the schedule keys are the same as the image size. Below, we present the steps of the algorithm in each round.

(I) The encryption algorithm applies a permutation P, on the pixel positions of the original image. This is done before the rounds start. Next, the xor operation is performed

between the string that results from the permutation and the first schedule key. Subsequently, the string that results from the xor operation is divided into 8-bit substrings, i.e., a byte. Finally, the substitution operation is applied to each of these bytes, using the first 8×8 S-box. The criteria used in the substitution operation are the same as in FIPS 197 [43]. Later, the permutation P, boxes, and schedule keys are generated.

(II) From rounds two to thirteen, the algorithm executes the following steps: it starts with an xor between the output of the previous round and the corresponding schedule key. Then, the substitution operation is performed with the corresponding 8×8 S-box.

(III) In round 14, the following steps are executed: first, the xor operation is applied between schedule key 14 and the output of round 13. Next, the result of the previous operation is subdivided into blocks of 8 bits, and the substitution process is then carried out with the last box. It is terminated with an xor operation with schedule key 15. This last result provides the encrypted image.

Regarding the construction of the permutation, the schedule keys and the boxes are shown in the next section.

3.5. Generation of the S-Boxes, Permutation, and Schedule Keys

The procedure for generating the 8×8 S-boxes is shown below:

(a) An integer C^1 is randomly obtained that satisfies $0 < C^1 < 2^{512}$. Subsequently, the point $C^1\alpha$ is calculated, where α is the primitive number. Let us denote the result $C^1\alpha = (w_1, w_2)$.

(b) In this investigation, the constant D_3 of Equation (25) is proposed. It has a value associated with the binary string $w_1 \parallel w_2$. Afterward, the operations $0.2881D_3e$ are performed.

(c) According to the result of section (b), the bits from the decimal point to the right are divided into blocks of 8 bits. Furthermore, it is clarified that an 8×8 S-box is a permutation of the 256 elements of the set $\{00, 01, \cdots ff\}$. The constants A_i of Equation (42) are computed, and then the permutation is obtained. In this order of ideas, the calculation of A_0 is done as follows: the first 8 bits after the decimal point are taken, and the integer associated with this string of bits is called a_0. Then, the following calculation is carried out: $A_0 = a_0 \mod 256$, such that $0 \leqq A_0 < 256$ holds. A_i is related to the i-th block of 8 bits to the right of the decimal point. This block has an associated integer value which we denote as a_i. So, $A_i = a_i \mod 256$ - i with $0 \leqq i < 255$, considering that $A_{255} = 0$.

(d) Once the A_i has been obtained, the algorithm outlined in Section 3.3 is used to generate the permutation. To get the other boxes, i.e., from two to fourteen, continue to shift to the right of the 8-bit decimal point and then perform the modular operation.

Regarding the generation of the permutation, the procedure is shown below.

(a) In the same way as before, an integer C^2 is randomly generated, that is in a range of $0 < C^2 < 2^{512}$.

(b) Once the value C^2 is obtained, the point $C^2\alpha$ is calculated, considering that α is the primitive number. Let us write the result of $C^2\alpha$ as (z_1, z_2). Then, the concatenation of the coordinates of (z_1, z_2) is performed; that is, $z_1 \parallel z_2$. The integer value associated with the binary string $z_1 \parallel z_2$ is assigned to the constant D_2 of the Equation (25).

(c) According to the previous step, the calculation $(0.4750 \times e)D_2$ is carried out. So, in this investigation, it is proposed to divide the binary string formed from the decimal point to the right into blocks of three bytes; that is, it starts with bytes 0, 1, 2. Let us refer to the non-negative integer associated with the binary string of the first three bytes as b_0; furthermore, let us denote the number of pixels in the image as l. With this information, the first constant, A_0, of Equation (42) is calculated as follows: $A_0 = b_0 \mod l - 0$. To obtain the constant A_i with $i > 0$, we will proceed as follows: i shifts one byte to the right of the decimal point, and the bytes $i, i + 1, i + 2$ are taken. In the same way as before, this 24-bit block has a non-negative integer, which is written as b_i. From here, the i-th constant is obtained as follows: $A_i = b_i \mod l - i$.

(d) When the constants indicated in Equation (42) are calculated, it is possible to generate a permutation as mentioned in Section 3.3.

On the other side, the previous steps are essentially described below. A positive integer C^1 is chosen, that satisfies the condition where it is less than the number of solutions (2^{512}). This value leads us to a point on the curve (w_1, w_2). The previous point generates the integer $D_3 = w_1 \parallel w_2$. From here, it is possible to execute the operation indicated in Equation (25). Blocks of one byte are taken to the right of the decimal point. Each byte can be interpreted as an integer and used to obtain the A_i constants in Equation (42). Subsequently, a permutation is obtained over an array of 256 positions, which leads us to a box.

Regarding the schedule keys (third aspect), the same calculations in items (a) and (b) are performed to obtain the permutation of bytes of the image. Then, the constant C^2 is used.

Subsequently, the decimal point to the right l pixels are obtained from the product $(0.4750 \times e)D_2$; that is, a binary string of the image size. This paper sets this string as the first schedule key, denoted as k_1. To generate the other schedule keys; that is, $k_2 \cdots k_{15}$ the following is done:

For k_i with $i > 1$, a one-byte left circular shift of the key k_{i-1} is performed.

In order to illustrate the point, the elliptic curve used in this investigation is shown below. Furthermore, it is pointed out that the proposed curve meets the conditions mentioned in Equations (3)–(5).

The values of p, q, a, b, k, as well as, the primitive element $\alpha = (x_1, x_2)$ are expressed next.

p = 988464ba59685284506433ccd3f83450166fda2d2ec7
109a5c0679434e9dfb46b3a447043b406c4115af9a2c7fdc17
bc9b6668f07d80d7142f534a1dc64ef400b9b2100acb691

q = 2621192e965a14a114190cf334fe0d14059bf68b4bb1
c42697019e50d3a77ed1ace911d9c1e6fa9ecb772f44670d2
9e05a69fc249b108ed06114d9e01b7662721ecf151ce2329

a = 31662dbf1d0c1691728e2c47e26720c3d0f760b216aa8
00eb153c54ae3e0c522345eb09

b = 308

k = 870eebe8cf19ece84593dd9deaec2ebab1380c94c240fe
8fc1d45836fff18114c42308e5aafef0ee4d1a643b179415eb
34d8b2118e51ad727b63efc5dba104179bcece5a0d7cb

On the other hand, the generator element $\alpha = (x_1, x_2)$ is presented below:

x_1 = 28b1f61561824dac022aa29d37df70295a2d7f34f696
5e032d85b35b6e4c8403a47922b96753ba338061a05eee5
30f5759043d58aa09d69ae8b2377b640c01e484ac14d27d
693

x_2 = 288189d9988f9d839ae797195f3a4b512b36773156af
fd0b64a5ed740c9ea059233eab4765397a0a5de87ea46a20
d208cf8988d433e4d703792e2f950ad6a0a631f0d424e6951

In another order of ideas, it can be seen that the points (w_1, w_2) and (z_1, z_2) are important in constructing the symmetric cryptosystem. So, in a secure communication scheme, for example, the PKI [44], the recipient only needs to know these points to develop the particular symmetric cryptosystem. In this sense, the sender can send the points mentioned above using the recipient's public key called Q. Later, the recipient using their private key can get (w_1, w_2) and (z_1, z_2). Furthermore, the sender can sign the message according to the Elliptic Curve Signature Algorithm (ECSA) [45] standard.

3.6. Images Used to Evaluate ICLEBF

Figure 1 shows the images used in this research to evaluate the encryption quality of the proposed cryptosystem. The size of the images is 512 × 512 pixels, according to the convention used in this kind of research work [46], although they can be of different dimensions.

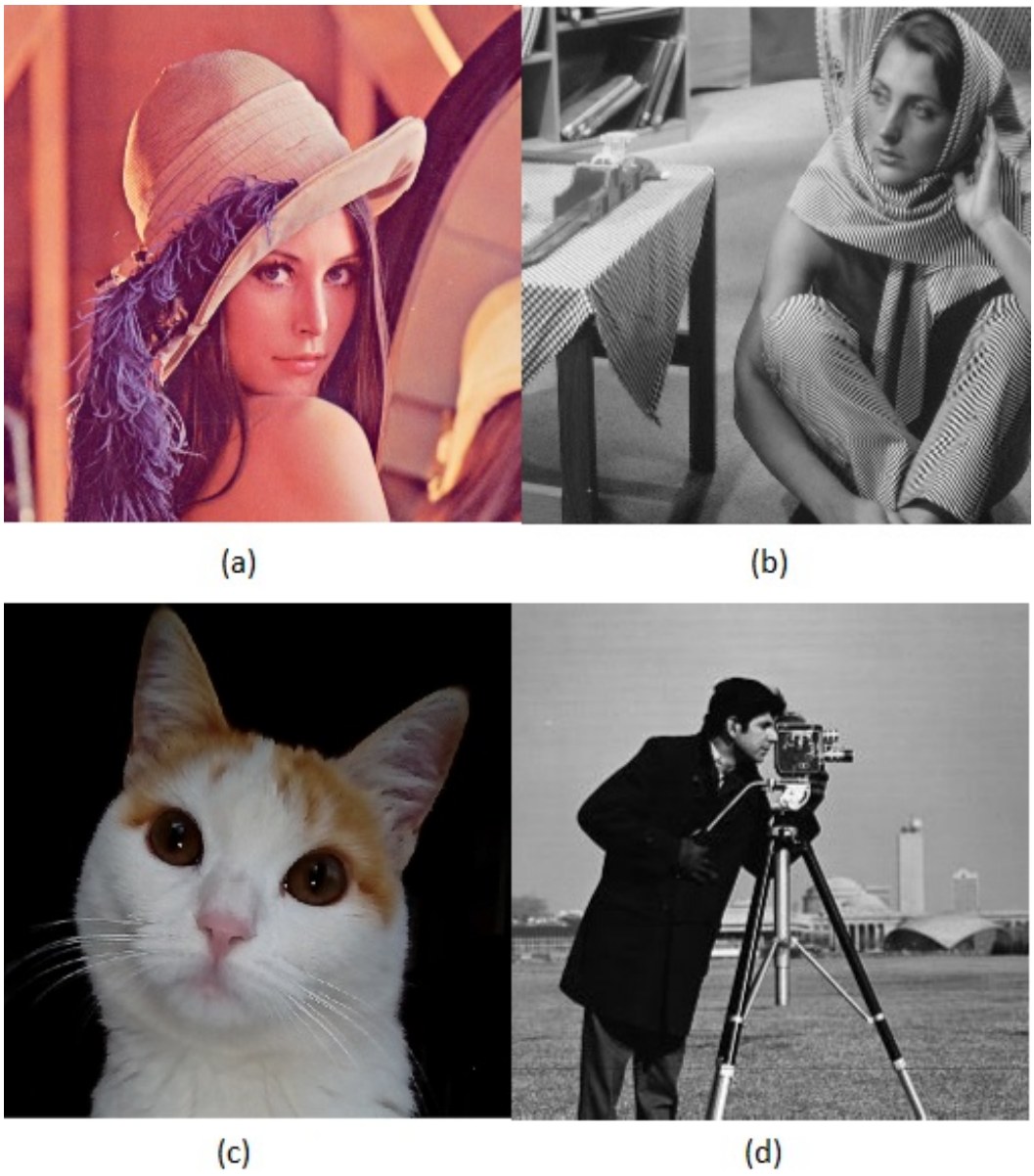

Figure 1. Images used for evaluating ICLEBF: (**a**) Lena, (**b**) Barbara, (**c**) Vicky, (**d**) Cameraman.

The Barbara and Cameraman images (Figure 1b and Figure 1d, respectively) are used to test the proposed encryption algorithm because, when using 256-gray-level images, there is a risk of poor-quality encryption if a secret-key cryptosystem is used. In fact, this is why AES is not used as a standard in image encryption, and the AES–CBC [47] cryptosystem is instead employed. Furthermore, in those images, parts are entirely white, and in the other image, parts are completely black.

On the other hand, Figure 1a is widely known in the encryption field; the Lena image. Furthermore, in this research, the image of Vicky in Figure 1c is used, and both images are in color, i.e., the three primary colors appear, red, green, and blue, with 256 levels for each one.

To conclude this section, it is noted that Figure 1c is encrypted with AES–CBC, and then an occlusion noise damage of 40% of the encrypted figure size is applied. This is later decrypted. The previous result is compared with that obtained when the same procedure is carried out, except that Figure 1c is now encrypted with the ICLEBF algorithm. Finally, in the "Result" section, the comparison is shown.

4. Damage in Encrypted Images

This work employs five types of noise and applies them to images encrypted with ICLEBF. These noises are the following: χ^2, Gaussian, occlusion, additive and multiplicative; considering that in this research, the noise χ^2 is proposed. On the other hand, the parameter Similarity Parameter (SP) defined above is proposed to evaluate the damage in sharpness. In addition, a median filter 5×5 is applied to complement the process.

4.1. Noise Generated by the Variable χ^2

This section begins with a description of the noise χ^2, that is based on the random variable $\chi^2 = \sum_{i=1}^{k} \frac{(o_i - \exp)^2}{\exp}$. Considering that the noise χ^2 is presented in Section 2 and using the central limit theorem, this noise variable is distributed as a normal variable, with a mean $\mu = 255$ and a standard deviation $\sigma = 22.58$.

Furthermore, the images damaged in this research have two domains: spatial and frequency. The process begins with the choice of n points at random in the spatial domain of the encrypted image. These points have an associated intensity in the frequency domain, which we call I_c; furthermore, it satisfies $0 \leq I_c \leq 255$. The subscript indicates the primary color type.

Once the n points, denoted as (x, y), have been chosen for each color, a value $z_c \sim \mathrm{N}(0, 1)$ is randomly chosen. Subsequently, we calculate the value I'_c according to Equation (44).

$$I'_c(x, y) = 255 + z_c(x, y)42.5 \tag{44}$$

The next step is to assign an integer value to the variable I'_c, i.e., this variable is discretized. In this sense, we will use the symbols $\lfloor\ \rfloor$ and $\lceil\ \rceil$ as follows: when the decimal part of I'_c is less than or equal to 0.5, the integer part is taken I'_c, which is denoted as $\lfloor I'_c \rfloor$. Otherwise, when the decimal fraction is greater than 0.5, the integer part plus one of I'_c is taken. The above is denoted as $\lceil I'_c \rceil$.

In this work, the discretized value of I'_c is denoted as I'_{dc} and is calculated according to Equation (45).

$$I'_{dc}(x, y) = \lfloor \lceil 255 + z_c(x, y)42.5 \rceil \rfloor \mod 256 \tag{45}$$

It is necessary to replace the value of I_c with I'_{dc} to apply the noise to the encrypted image. Furthermore, note that the symbols $\lfloor\ \rfloor$ or $\lceil\ \rceil$ in Equation (45) are used as appropriate. Before concluding this section, it is important to mention that the vast majority of the intensities (95%) are replaced by values that fall within the following ranges: [0, 84] or [170, 255]; i.e., by extreme values.

4.2. Additive and Multiplicative Noises

In the same way, as in the previous section, there are two domains. In this sense, n points (x, y) are randomly chosen from the spatial domain, that is, from the encrypted image; each has an associated intensity I_c that complies with $0 \leqq I_c \leqq 255$.

In the case of additive noise, for each point (x, y) and color, an integer $\gamma(x, y)$ is chosen at random, and then the calculations indicated in Equation (46) are done. To apply the additive noise, proceed as follows: the value of I_c is replaced by I'_c, obtained in Equation (46).

$$I'_c(x, y) = [I_c(x_1, x_2) + \gamma(x_1, x_2)] \mod 256 \tag{46}$$

The procedure of the multiplicative noise is similar to the additive one. In fact, the value of I'_c is obtained according to Equation (47). Then, to apply the multiplicative noise shown in Equation (47), the value of I_c is replaced by I'_c.

$$I'_c(x, y) = [I_c(x_1, x_2) \times \gamma(x_1, x_2)] \mod 256 \tag{47}$$

4.3. Gaussian Noise

This part analyzes the application of Gaussian noise, which leads to the random variable x with a standard normal distribution, i.e., $x \sim \mathrm{N}(0, 1)$.

In this sense, in the spatial domain, n points (x_1, x_2) are randomly chosen according to the uniform distribution. These points also have an associated intensity I_c, which meets the following condition: $0 \leqq I_c \leqq 255$.

In this work, the intensity I'_c is calculated according to Equation (48) considering that $z \sim \mathrm{N}(0, 1)$. Furthermore, it is mentioned that the values of z are obtained with a standard normal distribution generator; that is, $z \sim \mathrm{N}(0, 1)$. In addition, the following rule applies: when the value of z generated with this standard normal distribution is less than -3, this takes the value $z = -3$. On the contrary, when the generated value is greater than 3, this takes the value $z = 3$. It follows that the range of z is $[-3, 3]$.

$$I'_c = 127.5 + z \times (42.5) \tag{48}$$

The symbols $\lfloor, \rfloor$ and $\lceil, \rceil$ are used to discretize the variable I'_c. In this sense, it proceeds as follows: when the decimal fraction of I'_c is less than or equal to 0.5, only the integer part is considered, and the above is denoted as $I_{dc} = \lfloor I'_c \rfloor$. On the other hand, if the decimal fraction is greater than 0.5, then the integer part plus one is taken, and this is denoted as $I_{dc} = \lceil I'_c \rceil$.

From here, it is proposed to apply the Gaussian noise to the encrypted image in the following way: the value of I_c is replaced by that of $I_{dc} = \lfloor I'_c \rfloor$ or $I_{dc} = \lceil I'_c \rceil$ according to the case. On the other hand, 95% of the substituted values are in the interval [42, 212]; i.e., centered around 127.5.

4.4. Occlusion Noise

The occlusion noise is applied in the following way: the intensity of all points of a concentric parallelogram is replaced by a single color, which in this investigation is a cherry color.

As can be seen, the above is equivalent to producing noise inside the concentric parallelogram. In order to clarify ideas, this procedure is illustrated in Figure 2.

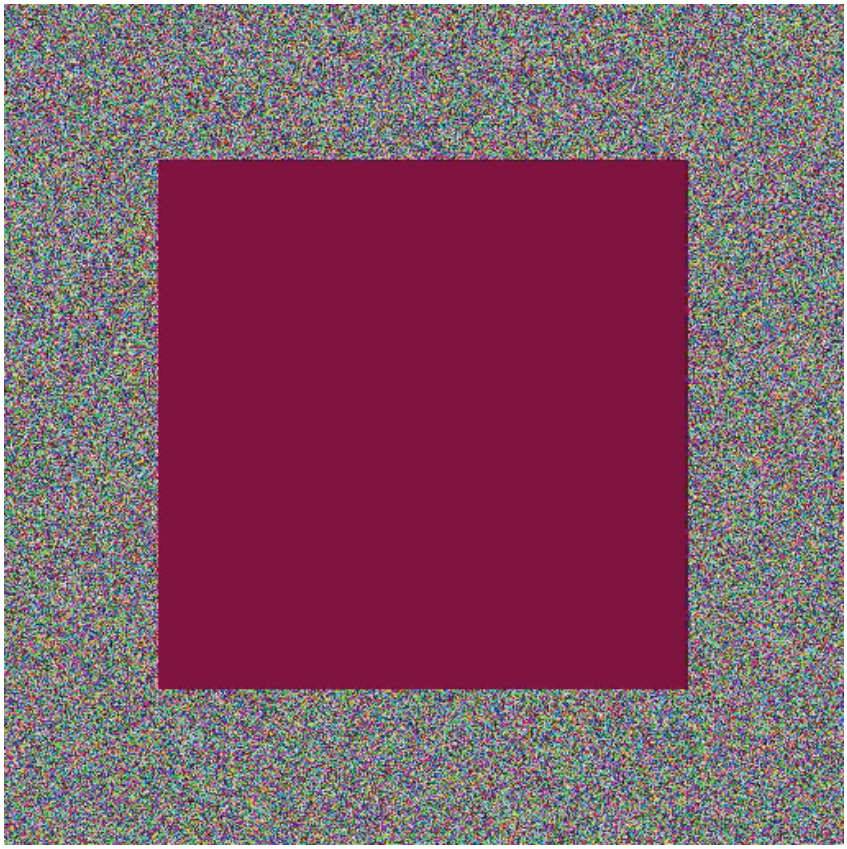

Figure 2. Occlusion noise in an encrypted image.

5. Results

First, we will show the results of encrypted images without damage and later the results when damaged. In addition, it starts with the correlation and entropy parameters. Subsequently, the NPCR, UACI, AC, energy, contrast, and homogeneity measurements are presented. Later, the parameters that apply hypothesis tests are described.

Figure 3 shows how the ICLEBF algorithm encrypts. In this sense, it is mentioned that regardless of whether the flat image (original) is in color or 256 levels of gray, the encrypted figure will always be in color. The encrypted image is Figure 1b (Barbara).

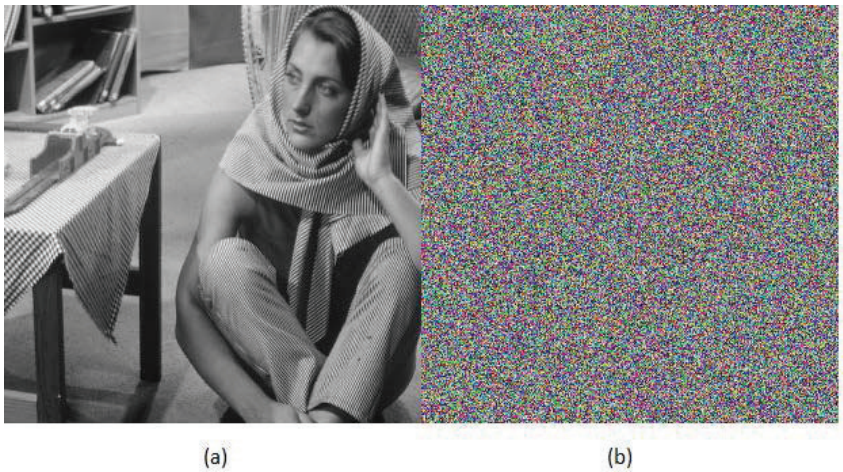

Figure 3. Barbara image (**a**) original and (**b**) ciphered with AICPBD.

5.1. Correlation and Entropy

Table 2 presents the results of the correlation when the test images of Figure 1 are encrypted.

Table 2. Correlation of the encrypted test images of Figure 1.

Color	Correlation	Lena	Barbara	Vicky	Cameraman
Red	Horizontal	0.0004	−0.0080	−0.0011	−0.0061
	Vertical	−0.0097	0.0086	0.0034	0.0009
	Diagonal	0.0069	−0.0034	0.0079	0.0133
Green	Horizontal	−0.0037	−0.0196	−0.0170	0.0014
	Vertical	−0.0052	0.0060	0.0006	0.0131
	Diagonal	0.0058	−0.0065	0.0174	0.0062
Blue	Horizontal	−0.0044	0.0198	−0.0037	0.0030
	Vertical	0.0116	−0.0021	−0.0019	−0.0012
	Diagonal	0.0009	−0.0020	0.0042	0.0146

Table 3 shows the entropy results. As pointed out previously, only results are presented in this part. Later, the corresponding analysis will be made.

Table 3. Entropy of the encrypted test images of Figure 1.

Color	Lena	Barbara	Vicky	Cameraman
Red	7.99919	7.99935	7.99919	7.99932
Green	7.99929	7.99925	7.99928	7.99926
Blue	7.99923	7.99935	7.99927	7.99947

Table 4 shows a comparative results of Lena entropy with other cryptosystems.

Table 4. Entropy analysis of Lena Figure 1a.

Color	ICLEBF System	[48]	[49]	[50]
Red	7.9992	7.9921	7.9987	7.9972
Green	7.9993	7.9917	7.9991	7.9973
Blue	7.9992	7.9972	7.9983	7.9972

5.2. Results of NPCR, UACI, AC, Energy, Contrast and Homogeneity

Tables 5–7 present the results of NPCR, UACI and AC, respectively. On the other hand, the energy, contrast and homogeneity are presented in Tables 8–10.

Table 5. NPCR of the test images after encryption.

Color	Lena	Barbara	Vicky	Cameraman
Red	99.609	99.606	99.602	99.603
Green	99.614	99.608	99.598	99.620
Blue	99.613	99.604	99.608	99.620

Table 6. UACI of the test images after encryption.

Color	Lena	Barbara	Vicky	Cameraman
Red	33.414	33.437	33.478	33.486
Green	33.461	33.562	33.483	33.452
Blue	33.365	33.468	33.421	33.457

Table 7. AC of the test images after encryption.

Color	Lena	Barbara	Vicky	Cameraman
Red	49.997	49.994	50.003	49.996
Green	49.996	50.020	49.985	49.961
Blue	49.963	49.981	50.014	49.944

Table 8. Energy of Figure 1 images after encryption.

Color	Lena	Barbara	Vicky	Cameraman
Red	0.0156	0.0156	0.0156	0.0156
Green	0.0156	0.0156	0.0156	0.0155
Blue	0.0156	0.0156	0.0155	0.0156

Table 9. Contrast of Figure 1 images after encryption.

Color	Lena	Barbara	Vicky	Cameraman
Red	10.501	10.516	10.475	10.472
Green	10.504	10.450	10.514	10.538
Blue	10.526	10.494	10.503	10.503

Table 10. Homogeneity of Figure 1 images after encryption.

Color	Lena	Barbara	Vicky	Cameraman
Red	0.388	0.389	0.390	0.389
Green	0.389	0.389	0.389	0.388
Blue	0.389	0.388	0.389	0.389

5.3. Discrete Fourier Transform and Goodness-of-Fit Test

This part shows the parameters' results, including a statistical hypothesis test. Table 11 presents the measurements obtained when the parameter of the discrete Fourier transform is applied to the encrypted images of Figure 1, and Table 12 illustrates the values obtained when using the goodness-of-fit test in the encrypted figures of the four test images.

Table 11. The randomness measurement using the Discrete Fourier Transform (✓ Accept, x Reject), with $\alpha = 0.01$.

Color	Lena	Barbara	Vicky	Cameraman
Red	0.671/✓	0.978/✓	0.342/✓	0.093/✓
Green	0.368/✓	0.116/✓	0.737/✓	0.272/✓
Blue	0.191/✓	0.214/✓	0.182/✓	0.469/✓

Table 12. Results of the *Goodness-of-Fit* test (✓ Accept, x Reject), with $\alpha = 0.01$.

Color	Lena	Barbara	Vicky	Cameraman
Red	242.9/✓	256.3/✓	259.3/✓	243.9/✓
Green	252.7/✓	229.8/✓	254.6/✓	251.9/✓
Blue	287.5/✓	260.7/✓	264.2/✓	272.3/✓

5.4. Tests on Black or White Images

The purpose of conducting tests on entirely black or white images is because ICLEBF defines a symmetric cryptosystem. Subsequently, the encryption may not perform correctly. For this reason, the measurements of NPCR, UACI, and AC are carried out in the encrypted figures, one of the images in black and the other in white. In this sense, the results are reported in Table 13. Furthermore, the size of both images is set to 512×512 pixels.

Table 13. NPCR, UACI and AC values for the completely black and completely white images.

Parameter	Color	Black Image	White Image
NPCR	Red	99.610	99.588
	Green	99.606	99.605
	Blue	99.603	99.627
UACI	Red	33.429	33.384
	Green	33.428	33.520
	Blue	33.480	33.410
AC	Red	50.039	50.005
	Green	49.950	49.989
	Blue	49.986	50.006

5.5. Result of Encrypted Images with Noise

We start this section by showing Figure 4, which has three images. The first, Figure 4a presents Barbara's flat (original) image. In the second one, Figure 4b, Barbara's image is encrypted with the AES–CBC algorithm, and then multiplicative noise is applied to the encrypted figure at 40% of its size. Finally, in the last Figure 4c, Barbara is encrypted with the ICLEBF algorithm, then multiplicative noise is applied to 40% of the encrypted figure and it is subsequently decrypted.

On the other hand, Figure 5 illustrates the case of the Vicky image shown in Figure 1c, which is encrypted with AES–CBC (Figure 5a), and then occlusion noise is applied to 40% of the encrypted image (Figure 5b). In this sense, Figure 6 shows the case in which the Vicky image is encrypted with the ICLEBF algorithm, and then the occlusion noise is applied to 40% of the encrypted figure, as shown in Figure 6a. It is later deciphered, resulting in Figure 6b.

Regarding the application of the median filter of 5×5 to complement the procedure, the deciphered images with noise are evaluated using the SP parameter to know the degree of improvement in sharpness. It is observed in Figure 7b the improvement of the sharpness of Vicky's image when the median filter 5×5 is applied to the damaged image. It is also important to comment that the Vicky image is encrypted with the ICLEBF algorithm. Furthermore, in Table 14 the sharpness evaluation is shown based on the SP parameter results. Different damage sizes χ^2 are applied to the encrypted test images in this case. On the other hand, Table 15 shows the SP parameter results when five types of noise are applied from 40% of the size of the encrypted test images, and the filter 5×5 is used to improve sharpness.

(a) (b)

(c)

Figure 4. Flat image of Barbara (**a**). Decrypted image of Barbara when a multiplicative noise of size 40% is applied to a figure encrypted with AES–CBC (**b**). Decrypted image of Barbara when a multiplicative noise of size 40% is applied to a figure encrypted with ICLEBF (**c**).

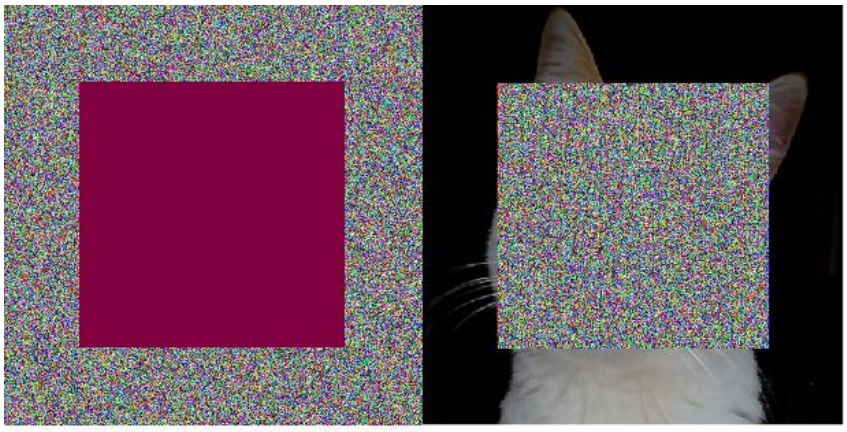

(a) (b)

Figure 5. Image (**a**) is the Vicky cat image ciphered of Figure 1c using AES–CBC with 40% occlusion damage and (**b**) is the deciphered image.

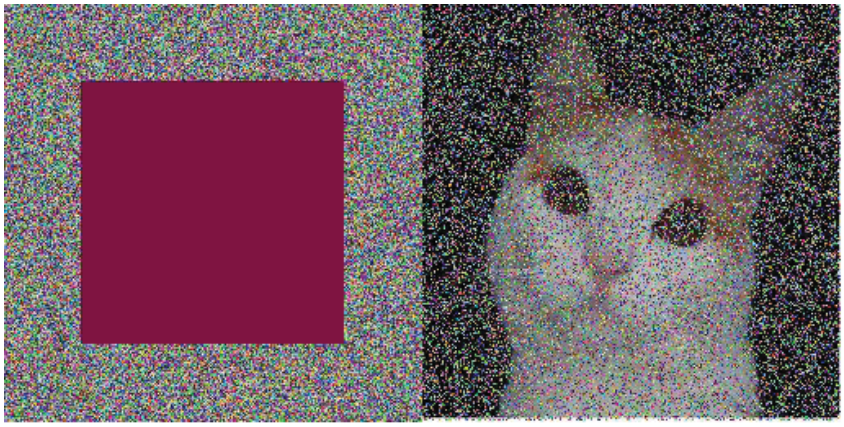

Figure 6. Vicky cat image (**a**) ciphered using ICLEBF with 40% occlusion damage and (**b**) is the deciphered image.

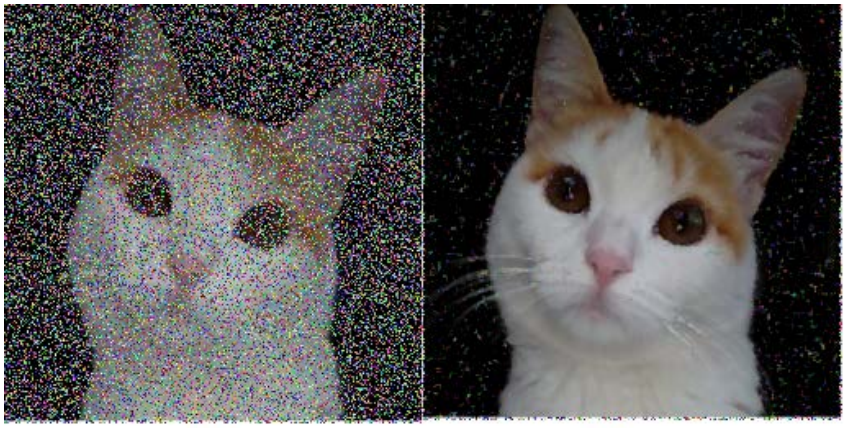

Figure 7. (**a**) The Vicky cat image deciphered with 40% occlusion noise, and (**b**) deciphered with noise and then median filter is applied.

Table 14. SP parameter for distinct noise size of the testing images after encryption, utilizing chi square damage.

Color	Size Noise	Lena	Barbara	Vicky	Cameraman
Red	20%	80.17	82.12	77.06	81.44
	30%	70.39	73.25	65.49	72.15
	40%	60.26	64.31	54.10	62.75
Green	20%	81.66	82.17	76.83	81.45
	30%	72.49	73.21	64.86	72.08
	40%	63.35	64.28	53.30	62.64
Blue	20%	83.43	82.12	76.47	81.34
	30%	75.14	73.15	64.68	72.12
	40%	66.92	64.33	52.89	62.80

Table 15. SP after a 5 × 5 median filter was applied to encrypted images with 40% damage from different noise sources.

Color	Noise Type	Lena	Barbara	Vicky	Cameraman
Red	Chi square	92.39	85.76	93.78	92.38
	Additive	92.36	85.81	93.76	92.49
	Multiplicative	92.54	85.93	94.11	92.57
	Gaussian	92.43	85.80	93.81	92.41
	Occlusion	92.59	85.84	93.86	92.47
Green	Chi square	90.71	85.85	93.61	92.47
	Additive	90.72	85.78	93.59	92.51
	Multiplicative	90.87	85.93	93.91	92.52
	Gaussian	90.76	85.80	93.75	92.40
	Occlusion	90.80	85.87	93.69	92.44
Blue	Chi square	91.94	85.85	93.42	92.48
	Additive	91.96	85.75	93.53	92.45
	Multiplicative	92.03	85.94	93.94	92.60
	Gaussian	91.93	85.82	93.63	92.40
	Occlusion	91.97	85.87	93.57	92.45

6. Discussion

Considering that the security of the ICLEBF algorithm is essential, we begin with possible attacks on the proposed cryptosystem. Later, an attack on the elliptic curve is observed, and then those that damage the encrypted figures.

In this order of ideas, the proposed cryptosystem attacks include the following: differential, linear, brute force, and algebraic. Regarding the differential attack, Tables 5, 6 and 7 show the results of the encrypted figures of the test images. It is observed that their values are in the desired range, i.e., NPCR around 99.6%, UACI values close to 33.3%, and AC around 50%. Therefore, it can be concluded that it resists differential attack. Regarding the linear attack, it is mentioned that the boxes are unknown since they are different in each encryption process, which means that the linear attack cannot be carried out as described in [51]. In addition, due to this same characteristic, the algebraic attack cannot be carried out either. Regarding the brute force attack, the following consideration is made: taking into account that when two points of the curve are known, the proposed cryptosystem can be built; furthermore, considering that the number of solutions is $q > 2^{512}$, it follows that the complexity of the problem is greater than $(2^{512})^2$. This is larger than the complexity of AES-256, and has not yet been solved by brute force [52].

The elliptic curve attack leads to the discrete logarithm problem, which consists of discovering the private key m when the public key Q is known. On the other hand, the discrete logarithm problem on the curve is equivalent to factoring a positive integer n in the RSA scheme [21]. In this sense, when the number of solutions q is a prime larger than 2^{512} (which is our case), the discrete logarithm problem is equivalent to factoring an n larger than 2^{15000}. The above is much larger than the application currently used in the RSA cryptosystem (2^{4096} [53]).

Two aspects are mentioned regarding the attack on encrypted images using noise: the first refers to a comparison of the proposed algorithm ICLEBF with the algorithm of the AES–CBC standard. Figures 5 and 6 show that ICLEBF better resists the occlusion attack because, after decrypting the damaged image, the original image is still visible. However, this is not the case with AES–CBC. Furthermore, the same happens in Figure 4. Figure 4b illustrates the case when Barbara's image is encrypted with AES–CBC, then corrupted with multiplicative noise, and deciphered. On the other hand, if the image is encrypted with ICLEBF and the same process is done as before, then Figure 4c is obtained.

The second aspect refers to the application of the median filter 5 × 5 to a decrypted image with corruption. In this sense, Figure 7b illustrates how a damaged image changes when the filter is applied. On the other hand, the IP parameter is applied to damaged

images. Table 14 presents the results concerning the extent to which the sharpness deteriorates when χ^2 noise is applied, at different sizes, to the encrypted images of Figure 1. Table 15 shows the extent to which the sharpness improves when the median filter 5×5 is applied to the damaged images. It is worth noting that the noise χ^2 of size 40% applied to the Vicky image provides a result of IP $\approx$ 53%. However, after applying the filter, as shown in Table 15, the IP parameter value is around 93%.

According to the results presented in Tables 2–12, it is affirmed that the image encryption is of sound quality because the color distribution in the encrypted images presents a random behavior. In this sense, the obtained quality is superior to those reported in some recent investigations [2,11,27] and are similar to [1,3,5]. Furthermore, according to the results in Table 13 related to the NPCR, UACI, and AC parameters of the encrypted black and white images, it is observed that they present suitable values [54]. On the other hand, in Table 14, the damages in the encrypted images are evaluated when the noise χ^2 of different sizes are applied to them. This measurement is carried out with the SP parameter. Table 15 evaluates the application of the 5×5 filter to images with different types of noise. In this sense, it is highlighted that the Vicky image with noise improves by more than 40% when the median filter is applied, according to the SP parameter.

Additionally, the algorithm was programmed in Java language, achieving an execution time for encryption/decryption of 0.3 s. This time was registered on a computer with an i9-10900K CPU with 10 cores and Windows 11 operating system.

7. Conclusions

This research proposes a symmetric cryptosystem, ICLEBF, to encrypt color images. The proposed cryptosystem is secure based on two aspects. The first aspect details that the boxes and permutations are dynamic; they are different in each encryption process. The second relates to the number of solutions q of the curve, which in this work is approximately 2^{562}. Futhermore, it bears certain advantages over existing cryptosystems, particularly over AES–CBC. Another essential issue to highlight regarding the ICLEBF cryptosystem is that in its construction, an asymmetric cryptosystem was utilized, the elliptic curve, making it possible to distribute its keys. Finally, the main reason behind proposing the current symmetric cryptosystem for the encryption of color images is that this type of cryptosystem will have less impact on quantum computers [18]. This is advantageous because, in this case, only the curve is required and not two cryptosystems, as in the PKI scheme. In addition, it is possible to sign the information. Furthermore, the encryption quality produces outstanding results according to 10 evaluation instruments. Finally, future quantum computers will have a drastic impact on current asymmetric algorithms [18], and thus future work will involve the sending of a seed via a post-quantum cryptosystem [18].

Author Contributions: Conceptualization, methodology, formal analysis, investigation, visualization, V.M.S.-G., R.F.-C. and M.A.C.-L.; writing—review and editing, data curation, software, validation, writing—original draft preparation, V.M.S.-G., R.F.-C., M.A.C.-L. and M.G.V.-C.; resources, supervision, project administration, funding acquisition, V.M.S.-G. All authors have read and agreed to the published version of the manuscript.

Funding: This work was funded in part by the economic support program of the Comisión de Operación y Fomento de Actividades Académicas (COFAA) and the Secretaría de Investigación y Posgrado (SIP) of the Instituto Politécnico Nacional under grant 20220154.

Institutional Review Board Statement: Not applicable.

Informed Consent Statement: Not applicable.

Data Availability Statement: The data that support the findings of this study are available from the corresponding author upon request.

Acknowledgments: The authors would like to thank the Instituto Politécnico Nacional of México (Secretaría Académica, Comisión de Operación y Fomento de Actividades Académicas COFAA, SIP, and CIDETEC), and the CONACyT (SNI) for their support in the development of this work.

Conflicts of Interest: The authors declare no conflict of interest.

Abbreviations

The following abbreviations are used in this manuscript:

ICLEBF	Image Cipher utilizing Lorenz Equation and a Bijective Function
NPCR	Number of Pixels Change Rate
UACI	Unified Average Changing Intensity
AC	Avalanche Criteria
SP	Similarity Parameter
SPN	Substitution Permutation Network
RSA	Rivest–Shamir–Adleman

References

1. Alexan, W.; ElBeltagy, M.; Aboshousha, A. RGB Image Encryption through Cellular Automata, S-Box and the Lorenz System. *Symmetry* **2022**, *14*, 443. [CrossRef]
2. Sani, R.H.; Behnia, S.; Akhshani, A. Creation of *S*-box based on a hierarchy of Julia sets: Image encryption approach. *Multidimens. Syst. Signal. Process.* **2022**, *33*, 39–62. [CrossRef]
3. Hayat, U.; Ullah, I.; Azam, N.A.; Azhar, S. A Novel Image Encryption Scheme Based on Elliptic Curves over Finite Rings. *Entropy* **2022**, *24*, 571. [CrossRef]
4. Murtaza, G.; Azam, N.A.; Hayat, U. Designing an Efficient and Highly Dynamic Substitution-Box Generator for Block Ciphers Based on Finite Elliptic Curves. *Secur. Commun. Netw.* **2021**, *2021*, 3367521. [CrossRef]
5. Zhou, S.; Zhao, Z.; Wang, X. Novel chaotic colour image cryptosystem with deep learning. *Chaos Solitons Fractals* **2022**, *161*, 112380. [CrossRef]
6. Li, T.; Yan, W.; Chi, Z. A new image encryption algorithm based on optimized Lorenz chaotic system. *Concurr. Comput.* **2022**, *34*, e5902. [CrossRef]
7. Ren, H.; Niu, S.; Chen, J.; Li, M.; Yue, Z. A Visually Secure Image Encryption Based on the Fractional Lorenz System and Compressive Sensing. *Fractal Fract.* **2022**, *6*, 302. [CrossRef]
8. Rashmi, P.; Supriya, M.C.; Hua, Q. Enhanced Lorenz-Chaotic Encryption Method for Partial Medical Image Encryption and Data Hiding in Big Data Healthcare. *Secur. Commun. Netw.* **2022**, *2022*, 9363377. [CrossRef]
9. Tang, M.; Zeng, G.; Yang, Y.; Chen, J. A hyperchaotic image encryption scheme based on the triple dislocation of the Liu and Lorenz system. *Optik* **2022**, *261*, 169133. [CrossRef]
10. Bhat, J.; Saqib, M.; Moon, A.H. Fuzzy extractor and chaos enhanced elliptic curve cryptography for image encryption and authentication. *Int. J. Syst. Assur. Eng. Manag.* **2022**, *13*, 697–712. [CrossRef]
11. Elsaid, S.A.; Alotaibi, E.R.; Alsaleh, S. A robust hybrid cryptosystem based on DNA and Hyperchaotic for images encryption. *Multimed. Tools Appl.* **2022**, *82*, 1995–2019. [CrossRef]
12. Li, M.; Wang, M.; Fan, H.; An, K.; Liu, G. A novel plaintext-related chaotic image encryption scheme with no additional plaintext information. *Chaos Solitons Fractals* **2022**, *158*, 111989. [CrossRef]
13. Ametepe, A.F.X.; Ahouandjinou, A.S.; Ezin, E.C. Robust encryption method based on AES-CBC using elliptic curves Diffie–Hellman to secure data in wireless sensor networks. *Wirel. Netw.* **2022**, *28*, 991–1001. [CrossRef]
14. Banik, A.; Laiphrakpam, D.S.; Agrawal, A.; Patgiri, R. Secret image encryption based on chaotic system and elliptic curve cryptography. *Digit. Signal Process* **2022**, *129*, 103639. [CrossRef]
15. Silva-García, V.M.; Flores-Carapia, R.; Rentería-Márquez, C.; Luna-Benoso, B.; Chimal-Eguía, J.C. Image cipher applications using the elliptical curve and chaos. *Int. J. Appl. Math. Comput. Sci.* **2020**, *30*, 377–391. [CrossRef]
16. Shen, C.; Panda, S.; Vogelstein, J.T. The Chi-Square Test of Distance Correlation. *J. Comput. Graph. Stat.* **2022**, *31*, 254–262. [CrossRef]
17. General de la Nación, A. Manual de digitalización de documentos. *Bol. Arch. General Nación* **2022**, *9*, 41–117.
18. Stinson, D.R.; Patterson, M. *Cryptography: Theory and Practice*, 4th ed.; CRC Press: Boca Raton, FL, USA, 2018; pp. 278–295.
19. Underwood, R.G. *Cryptography for Secure Encryption*, 1st ed.; Springer: Cham, Switzerland, 2022; pp. 271–296.
20. Zheng, Z. *Modern Cryptography*, 1st ed.; Springer: Singapore, 2022; Volume 1, pp. 229–251.
21. Silva-García, V.M.; Flores-Carapia, R.; González-Ramírez, M.D.; Vega-Alvarado, E.; Villarreal-Cervantes, M.G. Cryptosystem Based on the Elliptic Curve With a High Degree of Resistance to Damage on the Encrypted Images. *IEEE Access* **2020**, *8*, 218777–218792. [CrossRef]
22. Ali, F.; Rather, B.A.; Fatima, N.; Sarfraz, M.; Ullah, A.; Alharbi, K.A.M.; Dad, R. On the Topological Indices of Commuting Graphs for Finite Non-Abelian Groups. *Symmetry* **2022**, *14*, 1266. [CrossRef]
23. Aldaya, A.C.; Sarmiento, A.J.C.; Sánchez-Solano, S. SPA vulnerabilities of the binary extended Euclidean algorithm. *J. Cryptogr. Eng.* **2017**, *7*, 273–285. [CrossRef]

24. Cohen, S.D.; Kapetanakis, G.; Reis, L. The existence of $\mathbb{F}_q$-primitive points on curves using freeness. *Comptes Rendus Math.* **2022**, *360*, 641–652. [CrossRef]
25. Yu, J.; Li, C.; Song, X.; Guo, S.; Wang, E. Parallel Mixed Image Encryption and Extraction Algorithm Based on Compressed Sensing. *Entropy* **2021**, *23*, 278. [CrossRef] [PubMed]
26. Zeng, J.; Wang, C.; Ye, G. A Novel Hyperchaotic Image Encryption System Based on Particle Swarm Optimization Algorithm and Cellular Automata. *Secur. Commun. Netw.* **2021**, *2021*, 6675565. [CrossRef]
27. Chai, X.; Fu, J.; Gan, Z.; Lu, Y.; Zhang, Y. An image encryption scheme based on multi-objective optimization and block compressed sensing. *Nonlinear Dyn.* **2022**, *108*, 2671–2704. [CrossRef]
28. Shannon, C.E. A mathematical theory of communication. *Bell Syst. Tech. J.* **1948**, *27*, 379–423. [CrossRef]
29. Panchikkil, S.; Manikandan, V.; Zhang, Y.D. An efficient spatial transformation-based entropy retained reversible data hiding scheme in encrypted images. *Optik* **2022**, *261*, 169211. [CrossRef]
30. Kowalska, K.A.; Fogliano, D.; Coello, J.G. *On the Revision of NIST 800-22 Test Suites*; Cryptology ePrint Archive, Paper 2022/540; Crypta Labs: London, UK, 2022. Available online: https://eprint.iacr.org/2022/540 (accessed on 11 December 2022).
31. Liu, Z.; Shen, J.; Barfield, R.; Schwartz, J.; Baccarelli, A.A.; Lin, X. Large-Scale Hypothesis Testing for Causal Mediation Effects with Applications in Genome-wide Epigenetic Studies. *J. Am. Stat. Assoc.* **2022**, *117*, 67–81. [CrossRef]
32. Bourgade, P.; Mody, K.; Pain, M. Optimal Local Law and Central Limit Theorem for β-Ensembles. *Commun. Math. Phys.* **2022**, *390*, 1017–1079. [CrossRef]
33. Pandurangi Ramacharya, B.; Patil, M.R.; Keralkar, S. Fast partial image encryption with fuzzy logic and chaotic mapping. *Evol. Intel.* **2022**, *1*, 1–17. [CrossRef]
34. Arab, A.A.; Rostami, M.J.B.; Ghavami, B. An image encryption algorithm using the combination of chaotic maps. *Optik* **2022**, *261*, 169122. [CrossRef]
35. Poojary, A.; Kiran Kumar, V.; Nagesh, H. FPGA implementation novel lightweight MBRISI cipher. *J. Ambient. Intell. Humaniz. Comput.* **2022**, *1*, 1–13. [CrossRef]
36. Kiran, P.; Parameshachari, B. Resource Optimized Selective Image Encryption of Medical Images Using Multiple Chaotic Systems. *Microprocess. Microsyst.* **2022**, *91*, 104546. [CrossRef]
37. Iqbal, N.; Hanif, M.; Rehman, Z.U.; Zohaib, M. On the novel image encryption based on chaotic system and DNA computing. *Multimed. Tools Appl.* **2022**, *81*, 8107–8137. [CrossRef]
38. Asif, M.; Asamoah, J.K.K.; Hazzazi, M.M.; Alharbi, A.R.; Ashraf, M.U.; Alghamdi, A.M. A Novel Image Encryption Technique Based on Cyclic Codes over Galois Field. *Comput. Intell. Neurosci.* **2022**, *2022*, 1–9. [CrossRef]
39. Guo, S.; Wang, G.; Han, L.; Song, X.; Yang, W. COVID-19 CT image denoising algorithm based on adaptive threshold and optimized weighted median filter. *Biomed. Signal Process. Control* **2022**, *75*, 103552. [CrossRef] [PubMed]
40. Fink, E.; Clarke, P.; Spoerk, M.; Khinast, J. Unsupervised real-time evaluation of optical coherence tomography (OCT) images of solid oral dosage forms. *J. Real-Time Image Process.* **2022**, *19*, 881–892. [CrossRef]
41. Gallian, J.A. *Contemporary Abstract Algebra*, 10th ed.; CRC Press: Boca Raton, FL, USA, 2021; pp. 19–21.
42. Lone, M.A.; Qureshi, S. RGB image encryption based on symmetric keys using Arnold transform, 3D chaotic map and affine hill cipher. *Optik* **2022**, *260*, 168880. [CrossRef]
43. Shetty, N.P.; Muniyal, B.; Kaithi, R.R.; Yemma, S.C.R. Comparison of Encryption Techniques to Encrypt Private Parts of an Image. In *Proceedings of the Advances in Electrical and Computer Technologies*; Sengodan, T., Murugappan, M., Misra, S., Eds.; Springer Nature: Singapore, 2022; pp. 535–557. [CrossRef]
44. Chanda, S.; Luhach, A.K.; Alnumay, W.; Sengupta, I.; Sinha Roy, D. A lightweight device-level Public Key Infrastructure with DRAM based Physical Unclonable Function (PUF) for secure cyber physical systems. *Comput. Commun.* **2022**, *190*, 87–98. [CrossRef]
45. Yuvaraj, N.; Praghash, K.; Karthikeyan, T. Data Privacy Preservation and Trade-off Balance Between Privacy and Utility Using Deep Adaptive Clustering and Elliptic Curve Digital Signature Algorithm. *Wirel. Pers. Commun.* **2022**, *124*, 655–670. [CrossRef]
46. Chai, X.; Wu, H.; Gan, Z.; Han, D.; Zhang, Y.; Chen, Y. An efficient approach for encrypting double color images into a visually meaningful cipher image using 2D compressive sensing. *Inf. Sci.* **2021**, *556*, 305–340. [CrossRef]
47. Zhang, Y.; Chen, A.; Chen, B. A unified improvement of the AES algorithm. *Multimed. Tools Appl.* **2022**, *81*, 18875–18895. [CrossRef]
48. Feixiang, Z.; Mingzhe, L.; Kun, W.; Hong, Z. Color image encryption via Hénon-zigzag map and chaotic restricted Boltzmann machine over Blockchain. *Opt. Laser Technol.* **2021**, *135*, 106610. [CrossRef]
49. Xingyuan, W.; Junjian, Z.; Guanghui, C. An image encryption algorithm based on ZigZag transform and LL compound chaotic system. *Opt. Laser Technol.* **2019**, *119*, 105581. [CrossRef]
50. Yaghouti Niyat, A.; Moattar, M.H.; Niazi Torshiz, M. Color image encryption based on hybrid hyper-chaotic system and cellular automata. *Opt. Lasers Eng.* **2017**, *90*, 225–237. [CrossRef]
51. Liu, X.; Tong, X.; Wang, Z.; Zhang, M. Uniform non-degeneracy discrete chaotic system and its application in image encryption. *Nonlinear Dyn.* **2022**, *108*, 653–682. [CrossRef]
52. Lin, C.H.; Hu, G.H.; Chan, C.Y.; Yan, J.J. Chaos-Based Synchronized Dynamic Keys and Their Application to Image Encryption with an Improved AES Algorithm. *Appl. Sci.* **2021**, *11*, 1329. [CrossRef]

53. Yarom, Y.; Genkin, D.; Heninger, N. CacheBleed: A timing attack on OpenSSL constant-time RSA. *J. Cryptogr. Eng.* **2017**, *7*, 99–112. [CrossRef]
54. K.U., S.; Mohamed, A. A novel image encryption scheme using both pixel level and bit level permutation with chaotic map. *Appl. Soft Comput.* **2020**, *90*, 106162. [CrossRef]